Twinned-serrated chip formation with minor shear bands in ultra-precision micro-cutting of bulk metallic glass

Sau Yee Chau[1], **Suet To**[1,] ***, Zhanwen Sun**[2], **Hongbing Wu**[3]

[1] State Key Laboratory of Ultra-precision Machining Technology, Department of Industrial and Systems Engineering, The Hong Kong Polytechnic University, Hong Kong, P.R. China

[2] State Key Laboratory of Precision Electronic Manufacturing Technology and Equipment, Guangdong University of Technology, Guangzhou, China

[3] College of Mechanical and Energy Engineering, Ningbo Institute of Technology, Zhejiang University, Ningbo, P.R. China

* E-mail: SandyTo@polyu.edu.hk,

Tel: +852-2766-6587, Fax: +852-2764-7657

Abstract: Bulk metallic glasses (BMGs) have unique properties due to their amorphous atomic structure such as excellent mechanical and thermal performances, BMGs are considered to be promising materials for many engineering applications. However, it is important to investigate the cutting mechanisms of BMG in ultra-precision micro-cutting (UPMC). This study focuses on experimental and theoretical investigations on the chip formation in UPMC of BMG. It was firstly found that twinned-serrated chips (TSCs) generated in UPMC of BMG. The intrinsic cause is that BMG exhibits significant adiabatic effect, which was confirmed by a proposed finite element model. A series of ultra-precision micro-cutting tests have been carried out to verify the results of simulation and reveal the effect of rake angle on the cutting process of BMG. The simulation and experiment of chip formation proved that the adiabatic effect is the key factor to generate the serrated chips in the UPMC of BMG. In addition, there existed twined shear in one cyclic of each serrated chip. The comparison between simulation and experiment under the machining condition of different tool rake angles showed that the serrated chip and cutting force are sensitive to the rake angle of tool.

Keywords: Adiabatic effect; Bulk metallic glass; Twinned-serrated chip; Finite element modeling; Ultra-precision micro-cutting;

1. Introduction

Bulk metallic glass (BMG) exhibits a lot of excellent performances, such as high strength and hardness, large elastic limit and superior resistance to wear and corrosion, as compared with traditional metals [1]. Different from conventional amorphous alloys, BMG are generated at very low critical cooling rates. Therefore, BMG not only have

common properties of traditional glassy alloys, but also has its own characteristics. Due to its unique physical, chemical, and mechanical properties, it has received intensive and increasing interests. Machining is a commonly employed cost-effective process for generating a required shape. However, BMG is a difficult to machine material due to its low heat conductivity and high strength [2], which limit its applications. To improve its machinability, some research works have been carried out to study its machining mechanisms.

Huang and Yan [3] studied crystallization behaviors at the workpiece surface layer of Zr-based BMG during micro-electrical discharge machining, using a X-ray diffractometer and a laser micro-Raman spectroscopy. The surface crystallization layer was effectively removed by subsequent grinding using sintered polycrystalline diamond. The combination machining process is a promising method to fabricate micro-features on the BMG surfaces. Bakkal et al. [4] elaborated that machining induced oxidation and crystallization of Zr-based bulk metallic glass since cutting temperature was very high which was up to 2400-2700 K. Additionally, Jiang and Dai [5] found that the unique lamellar chips were formed in machining of bulk metallic glass. The lamellar structures generated during chip formation are the combined results from the self-sustained limit-cycle phenomenon in stress, free volume and temperature in the primary shear zone. Fujita [6] announced that the slipping off generation mechanism of lamellar chips was the reason for the excellent machinability in turning of Zr-based BMG. However, Bakkal [1] proposed that the cyclic shear band formation would deteriorate surface quality. Besides, the drilling performances of BMG have been studied extensively. Zhu [7] observed the serrated chip formation in drilling of Zr-based BMG. They found that the nano-crystals presented in drilling of Zr-based BMG and facilitated the chip serration formation. Bakkal [8, 9] reported that drilling BMG under high speed would yield a light emission of chip and severe tool wear. More importantly, there existed feasible spindle speed and feed rate for efficient drilling BMG. The serrated chip formation was the general characteristics in drilling BMG.

Furthermore, ultra-precision micro-cutting (UPMC) has been well established for the precision fabrication of mass production, providing sub-micrometric form accuracy and nanometric surface roughness [10]. As a potential material, much more attentions has been initially paid to UPMC of BMG. Chen [11] reported the nano-crystallization and serrated chip formation of the BMG frequently existed in UPMC, a mirror surface could not be easily achieved due to its viscous flow, which the lowest achievable surface roughness was only 100 nm. Han [12] discussed that the serrated chips formation in UPMC of BMG was due to inhomogeneous localized maximum shear stress in nano-scratching.

As discussed above, current research works on machining of BMG reveal that the machined surface of BMG usually characterized by crystallizes and its chips are uniquely serrated in nature. Chip formation is an important indicator for surface quality and tool wear in machining [3]. However, the intrinsic serrated chip formation mechanisms have not been fully understood. Motivated by this, in this study, a series of orthogonal cutting tests were carried out to study the unique chip formation in UPMC of BMG. The chip morphologies were observed by a scanning electron microscope and the cutting forces were measured by a cutting force measurement system. In addition, the effects of tool

rake angle on chip formation were discussed. Furthermore, finite element modelling (FEM) was employed for the orthogonal UPMC simulation to reveal its intrinsic mechanisms, since it is a well-known powerful tool to study the complex cutting mechanisms [13-16].

2. Experimental setup

The material bulk metallic glass ($Zr_{55}Cu_{30}Al_{10}Ni_5$) is used in this study. Round bars of $Zr_{55}Cu_{30}Al_{10}Ni_5$ ingots 5mm-in-diameter and 70mm-in-length were prepared by arc melting fumace with copper mould. The amorphous structure of as-cast Zr-based BMG was characterized by X-ray diffraction (RigakuSmartLab) with using CuKα radiation as shown in Fig.1. The physical properties of bulk metallic glass ($Zr_{55}Cu_{30}Al_{10}Ni_5$) are listed in Table 1. The quantities of each physical property shown in Table 1 with respecting to the temperature change is neglected in this study. The orthogonal UPMC tests of BMG were performed on a 4-axis ultra-precision machine Moore 350FG. The schematic and the experiment of the orthogonal UPMC are shown in Fig.2. The round bars of BMG ingots were polished into a rectangular prism with dimension 60 mm (length) x 1 mm (wide) x 4 mm (thick), the workpiece was mounted on a fixture for ultra-precision machine. In the UPMC test, the workpiece moved in the Z direction and the single point diamond tool was fixed in location. To measure cutting forces, a Kistler 9252A force transducer was mounted between the tool shank and the tool fixture with a pre-loaded force to sense the cutting forces. The signals of the cutting forces were recorded with a Tektronix TDS 774A digitizing oscilloscope after being pre-amplified by a charge amplifier. The sampling frequency was set at 1 MHz. And the chips' morphologies were observed by the scanning electron microscope (Hitachi TM3000). The detailed cutting parameters are listed in Table 2. The radius of the diamond tool measured by atomic force microscope is 20 nm.

Table 1 Physical properties of Bulk metallic glass at room temperature (300K)

Properties	Values
Density (kg/m^3)	8620
Hardness (HRC)	46
Elastic modulus (GPa)	85
Thermal conductivity (W/mK)	5.02
Specific heat capacity ($Jmol^{-1}K^{-1}$)	26.5
Poisson's ratio	0.376
Linear thermal expansion ($10^{-6}/^oC$)	6.5

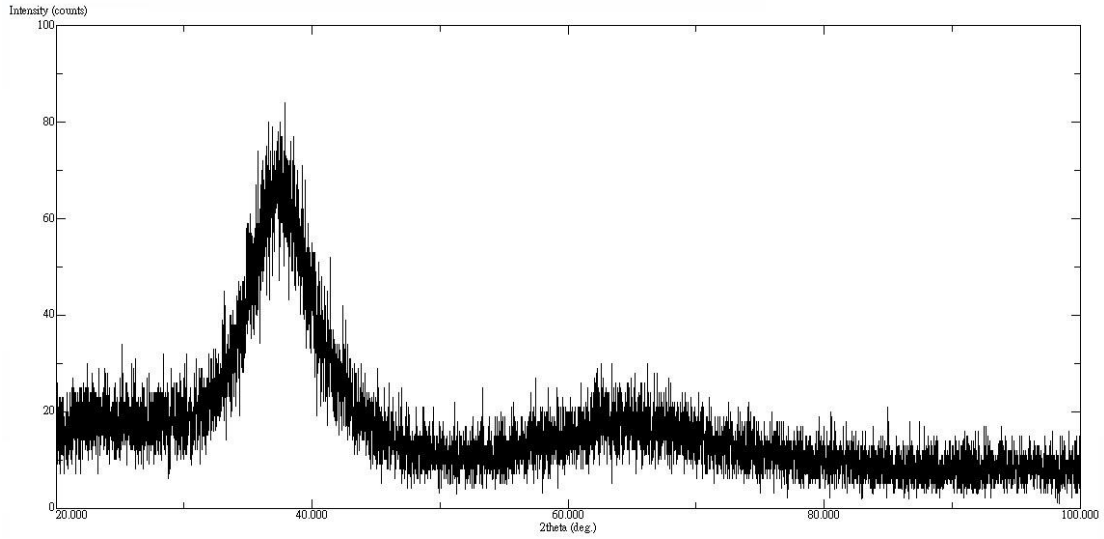

Figure 1. Characterization of as-cast $Zr_{55}Cu_{30}Al_{10}Ni_5$ bulk metallic glass by XRD.

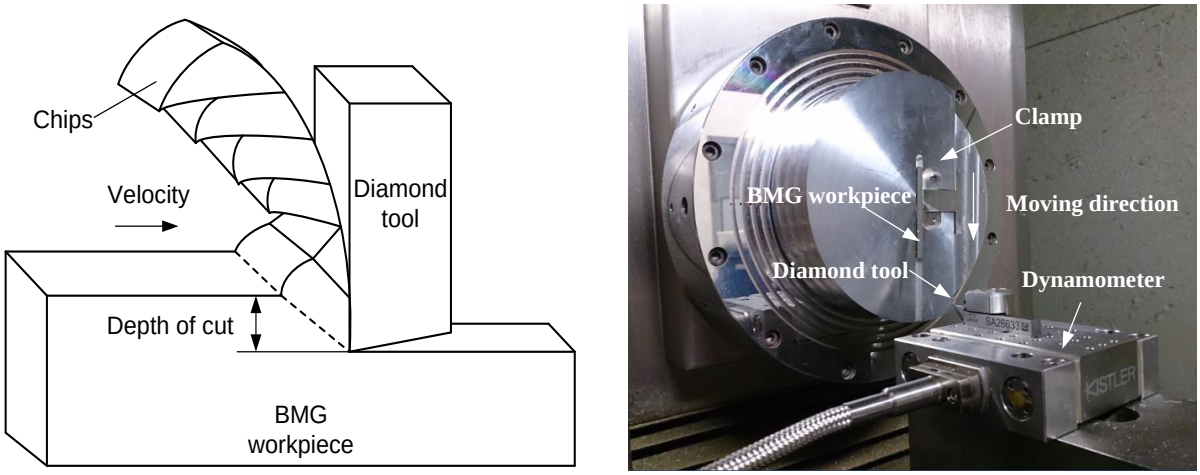

(a) Schematic of orthogonal UPMC (b) Equipment of orthogonal UPMC

Figure 2. Tests of UPMC for BMG

Table 2 Cutting parameters of UPMC

Parameters	Values
Cutting speed (mm/min)	100
Depth of cut (μm)	7
Tool type	Diamond tool
Rake angle of tool (°)	5, 0, -10, -25
Clearance angle of tool (°)	10
Cutting environment	Drying cutting

3. FEM in UPMC of BMG

To identify the material soft behavior due to the adiabatic effect in UPMC of BMG, the FEM was employed to obtain the information of chip formation. In this study, the software ABAQUS 6.12 was used to simulate the orthogonal UPMC of BMG. To reflect the adiabatic effect in UPMC, the analysis step "Dynamic, Explicit, adiabatic" was selected in the software. The orthogonal FEM for the UPMC of BMG is shown in Fig.3. In the simulation, the dimension of the part is 90 μm x 30 μm, and the part is meshed to 24,800 elements using the bilinear quadrangular element with reduced integration and hourglass control: CPE4R. In order to improve the accuracy, the mesh in the cutting layer was refined. The tool was set as a rigid-body with 1200 elements.

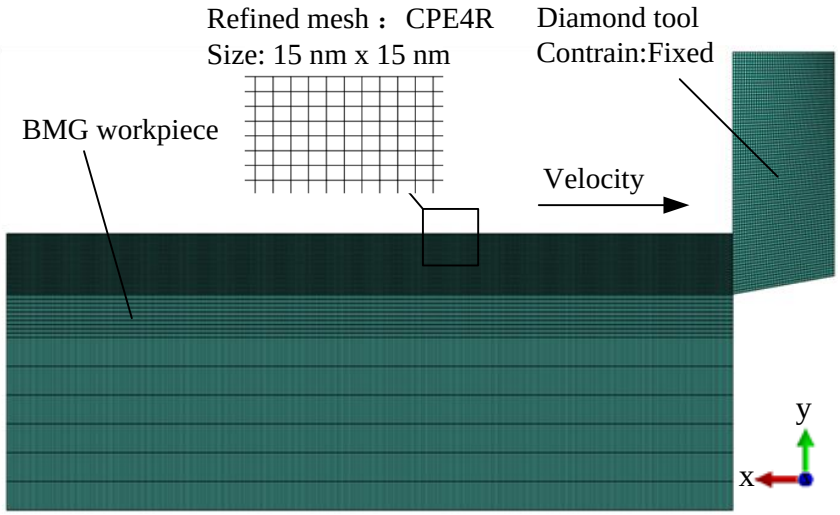

Figure 3. Orthogonal FEM in UPMC of BMG

The Johnson-Cook material law [17] was adopted in the simulation of UPMC for BMG, which was employed to study the phenomenon of BMG under the conditions of the large deformation, high strain rate and high temperature. The Johnson-Cook material model is expressed as follows:

$$\sigma = (A + B\varepsilon^{n})(1 + C\ln\dot{\varepsilon}^{*})(1 - T^{*m}) \quad (1)$$

where σ is the equivalent stress, and ε is the equivalent plastic strain. $\dot{\varepsilon}^{*} = \frac{\dot{\varepsilon}}{\dot{\varepsilon}_{ref}}$ is the relative equivalent plastic strain rate. $T^{*} = \frac{T - T_{ref}}{T_{m} - T_{ref}}$ is the homologous temperature, T_m is the melting temperature., and $\dot{\varepsilon}_{ref}$ and T_{ref} are the reference strain rate and the reference deformation temperature. A, B, n, C and m are material constants. A is the yield stress of the material under reference conditions, B is the strain hardening constant, n is the strain hardening coefficient, C is the strengthening coefficient of strain rate, and m is the thermal softening coefficient.

The Johnson-Cook parameters of Zr-based BMG were determined based on the deformation behavior of $Zr_{55}Cu_{30}Al_{10}Ni_5$ over a range of strain rates and temperature. Yin [18] conducted a series of uniaxial compression experiments to determine the stress-strain relationship for $Zr_{55}Cu_{30}Al_{10}Ni_5$ with different temperature values at constant strain rate and different strain rates under constant temperature. In this study, the reference strain rate, $\dot{\varepsilon}_{ref}$, and the

reference temperature, T_{ref}, were taken as 1x10^{-3} s^{-1} and 300K respectively.

Five material constants of Zr-based BMG can be determined independently. For determining A, B and n, the strain rate strengthening and thermal softening effect can be ignored. The Equation (1) can be modified as following form:

$$\sigma = (A + B\varepsilon^n) \tag{2}$$

After logarithm transformation, the Equation (2) can be described as following form:

$$\ln(\sigma - A) = n \ln \varepsilon + \ln B \tag{3}$$

By substituting the flow stress and strain values at the reference strain rate, 1x10^{-3} s^{-1}, and the reference temperature, 300K, into Equation (3), the material constants A, B and n were determined as 1702 MPa, 1381MPa and 0.82 respectively based on the linear relationship between $\ln(\sigma - A)$ and $\ln \varepsilon$.

For determining material constant C, the Equation (1) can be described as following at the deformation condition, $T = T_{ref}$ and $\dot{\varepsilon} = \dot{\varepsilon}_{ref}$:

$$\frac{\sigma}{\sigma_a} - 1 = C \ln \dot{\varepsilon}^* \tag{4}$$

where σ_a is the stress at $T = T_{ref}$, $\dot{\varepsilon} = \dot{\varepsilon}_{ref}$ and C is undetermined constant.

By substituting the stress values at three strain rates, 1x10^{-2}, 1x10^{-3} and 1x10^{-4}, at constant temperature, $T = T_{ref}$, into Equation (4), the material constant C was determined as 0.032 using curve fitting.

For determining material constant m, the Equation (1) can be described as following at a constant strain rate, $\dot{\varepsilon} = \dot{\varepsilon}_{ref}$:

$$\frac{\sigma}{\sigma_b} = 1 - T^{*m} \tag{5}$$

After logarithm transformation, the Equation (5) can be described as following form:

$$\ln(1 - \frac{\sigma}{\sigma_b}) = m \ln T^* \tag{6}$$

where σ_b is the stress at $T = T_{ref}$ and $\dot{\varepsilon} = \dot{\varepsilon}_{ref}$

By substituting the stress values at three temperature, 678K, 698K and 718K, at constant strain rate, $\dot{\varepsilon} = \dot{\varepsilon}_{ref}$, into Equation (6), the material constant m was determined as 6.88 using curve fitting.

The Johnson-Cook parameters of BMG were summarized in Table 3.

Table 3 Johnson-Cook material constitutive model parameters of BMG

A (MPa)	B (MPa)	n	C	M	T_{ref} (K)	T_m (K)
1702	1381	0.82	0.032	6.88	300	932

To simulate the chip separation from workpiece in UPMC, the Johnson-Cook failure model [19] was applied. The Johnson-Cook failure model is based on a hypothesis that the fracture occurred when the value of the plastics stain at element integration point reaches to a critical value. The failure is assumed to occur when damage parameter D exceeds 1. The Johnson-Cook failure model can be written as follows:

$$\varepsilon_f = \left[D_1 + D_2 \exp\left(D_3\left(\frac{\sigma_m}{\sigma_{eq}}\right)\right)\right]\left[1 + D_4 In\left(\dot{\varepsilon}_p{}^*\right)\right][1 + D_5 T^*] \tag{7}$$

where ε_f is the equivalent strain at failure, D_1 to D_5 are the damage model constants, σ_m is the mean stress, σ_{eq} is the equivalent stress, $\dot{\varepsilon}_p{}^* = \frac{\dot{\varepsilon}_p}{\dot{\varepsilon}_{ref}}$ is the relative equivalent plastic strain rate.

The damage parameter D is defined based on a cumulative law as follows:

$$D = \sum \frac{\Delta\varepsilon}{\varepsilon_f} \tag{8}$$

where $\Delta\varepsilon$ is the accumulated increment of equivalent plastic strain. The value of JC damage parameters used for the present study are specified in table 4.

Table 4 Johnson-Cook damage model parameters of BMG

D_1	D_2	D_3	D_4	D_5
-0.09	2.5	-0.5	0.002	2

To reflect the real thermal-mechanical behavior of BMG in UPMC, the scientific thermal-mechanical model needs to be established. The heat in the shear band zone generated by the deformation of BMG cannot be transferred effectively due to the low heat conductivity and high strain rate in UPMC, so, an adiabatic model was established in the simulation. Adiabatic thermal-stress analysis is typically used to simulate high strain rate processes involving large amounts of inelastic strain, where the heating of the material caused by its deformation is an important effect because of temperature-dependent material properties. An increase amount of temperature is calculated directly at the material integration points according to an increase in the adiabatic thermal energy caused by inelastic deformation; temperature is not a degree of freedom in the simulation. No allowance is made for the heat conduction in an adiabatic analysis. In the adiabatic analysis, plastic straining gives rise to a heat flux per unit volume of:

$$r^{pl} = \eta\sigma : \dot{\varepsilon}^{pl} \tag{9}$$

where r^{pl} is the heat flux added into the thermal energy balance, η is the user-specified inelastic heat fraction, σ is the stress, and $\dot{\varepsilon}^{pl}$ is the rate of plastic straining. The heat equation solved at each integration point is

$$\rho c(\theta)\dot{\theta} = r^{pl} \tag{10}$$

where ρ is the material density and $c(\theta)$ is the specific heat.

A real reflection of coupling contact features between the tool and chip interface can guarantee the accuracy of simulation. The modified Coulomb friction model has been used in the simulation. The average value of friction coefficient is set to be 0.2 in the simulation.

4. Results and discussion

4.1 Twinned-serrated chip formation

Fig.4 is the evolution process of the twinned shear in one serrated chip with the stress and temperature of the primary shear band in the UPMC of BMG. In Fig. 4a, the stress and temperature of primary shear band began to increase due to the material deformation in the shear zone. As shown in Fig.4b, the heat of deformation cannot be transferred effectively and the temperature in the adiabatic shear band reached the peak under the feed movement of the tool, so the chip began to flow because of the material thermal soften effect and the stress in the adiabatic shear band fall rapidly. The stress in the shear band is much less than outside, while the temperature shear band is much higher than outside. In the same time, a serrated chip began to form. But there existed one interesting phenomenon and the twinned minor shear appeared in Fig.4c. Whereafter, the twinned minor shear zone blended together with the first serrated chip due to the press of tool. Then the second cycle of serrated chip began to form.

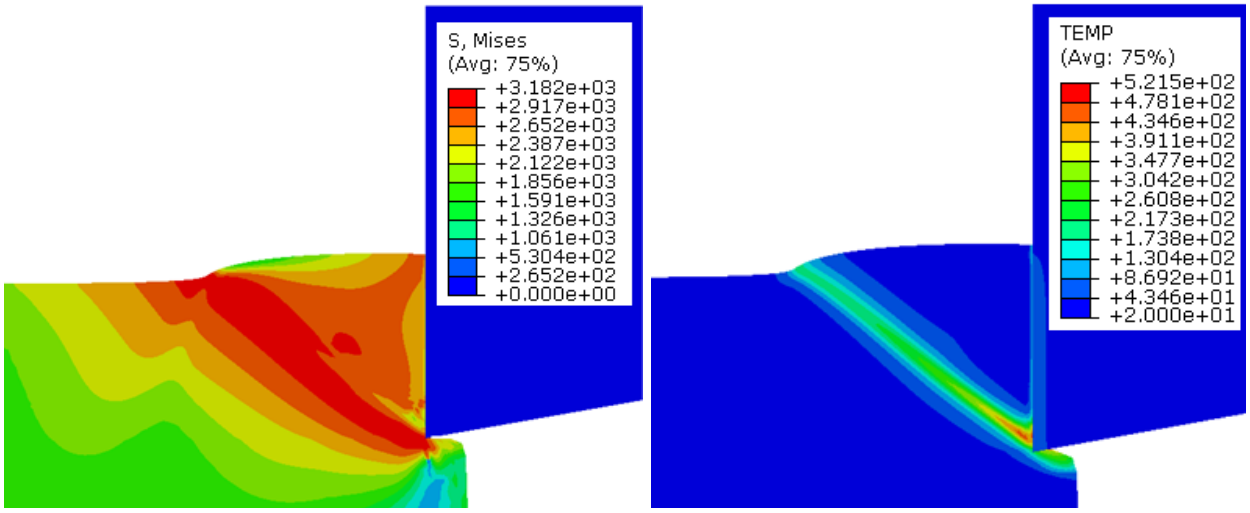

(a1) Stress distribution (a2) Temperature distribution

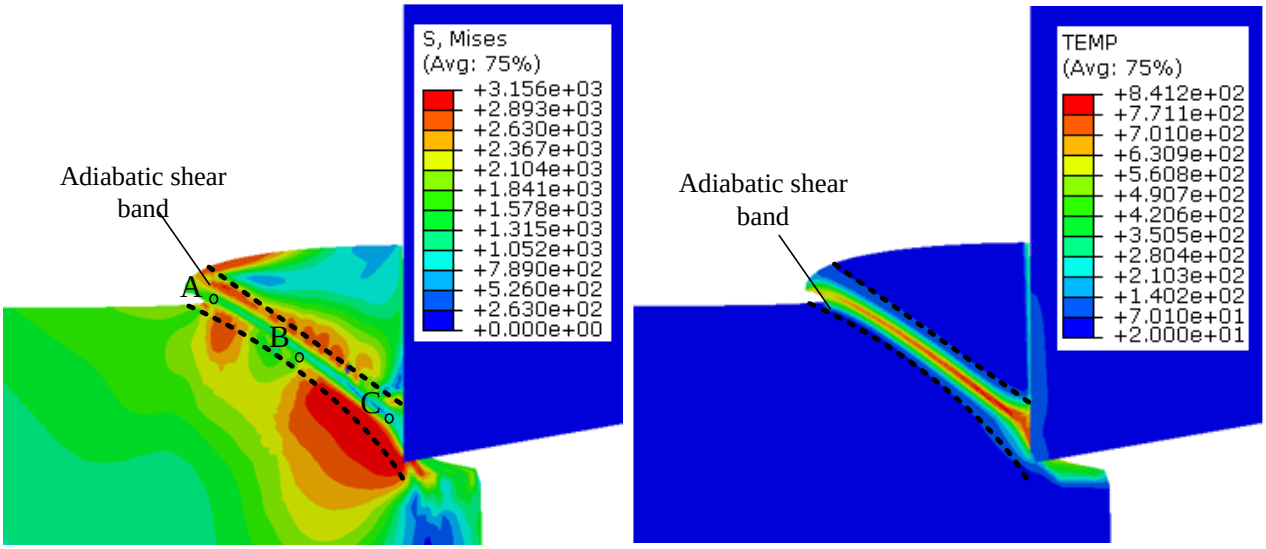

(b1) Stress distribution (b2) Temperature distribution

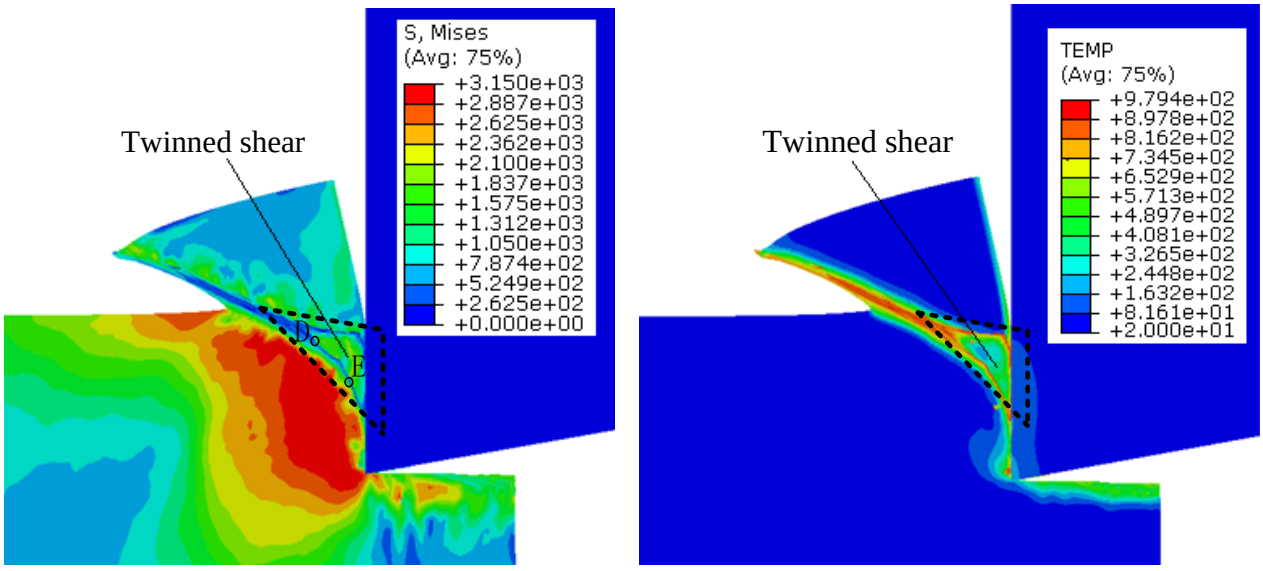

(c1) Stress distribution (c2) Temperature distribution

Figure 4. Simulation results on the formation of twinned serrated chip with the change of stress and temperature in

shear bands of BMG (UPMC: Rake angle 0°, cutting speed 100 mm/min)

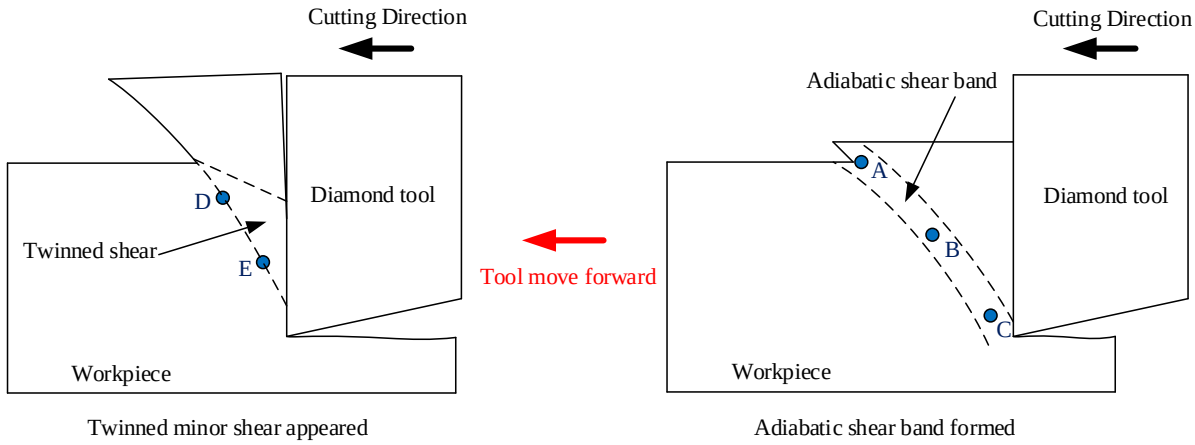

Figure 5. Equivalent points in the formation of one serrated chip

To reveal the change of stress and temperature at the shear band in UPMC of BMG, the points A,B and C in the primary adiabatic shear band, and the points D and E in the twinned shear band were selected. The locations of the five points are shown in Fig.5. Fig.6 is the changes in stress and temperature at the five points A, B, C, D and E during the formation of one serrated chip. It can be seen clearly that there are three stages in the formation cycle of one serrated chip: Elastic deformation, Plastic deformation and shear-fracture. During the three stages, the stress and temperature of the five points in the shear band began to increase, then the stress reached the peak and the material began to soften and flow. Locations A, B and C in the primary shear band began to shear firstly, then the stress decreased quickly and the temperature reached the peak. Whereafter, D and E began to shear and the twinned shear occurred, then the temperature of D, E reached the peak. The whole cycle of serrated chip finished. From the change tendency of stress and temperature at the five points, it proved fully that there existed the twinned shear in one cycle of each serrated chip.

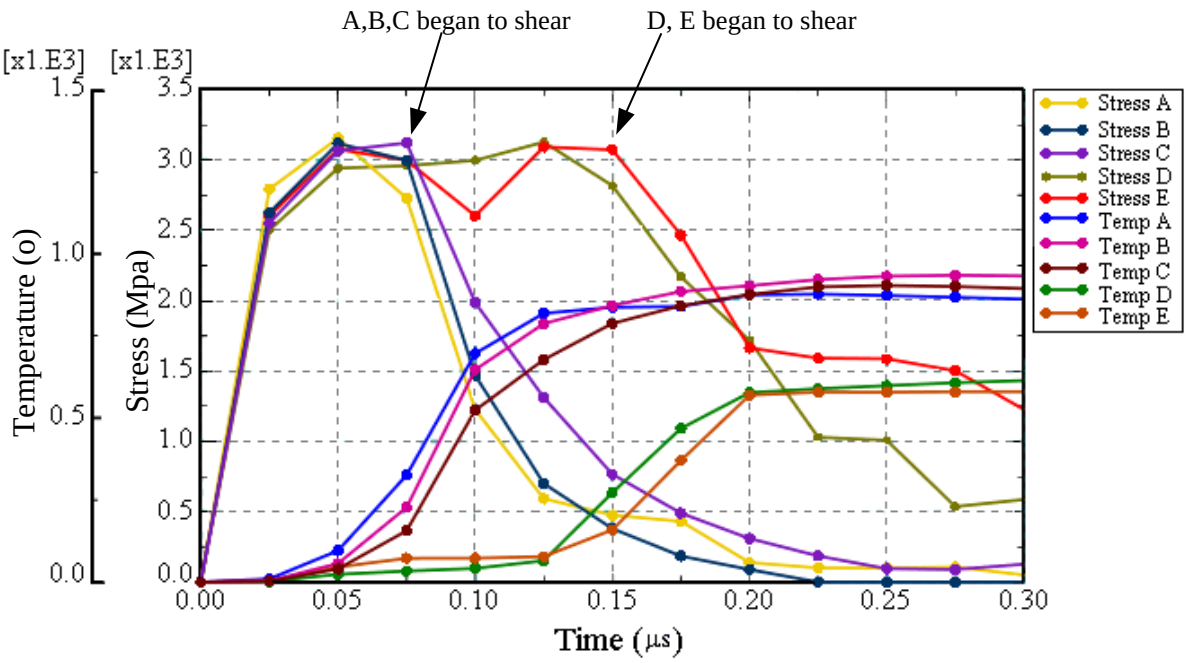

Figure 6. Change of stress and temperature at element A, B and C in the adiabatic shear band during the formation of one serrated chip

The primary cutting force curve of BMG in simulation and experiment are shown in Fig.7. From the Fig.7, it can be seen clearly that the cutting force fluctuates with the formation of the serrated chips. Different from the common cutting forces featuring orderly separated zigzag shapes observed in diamond cutting of other materials, the cutting forces shown in Fig. 7 are characterized twined minor shear phenomenon in each cycle of each serrated chip formation, which indicates a different material removal mechanism. Specifically, in diamond cutting of BMG, each zigzag cycle includes two separate crests, namely a big crest followed by a small one, which indicates that each chip formation for BMG has a two-step cutting behavior.

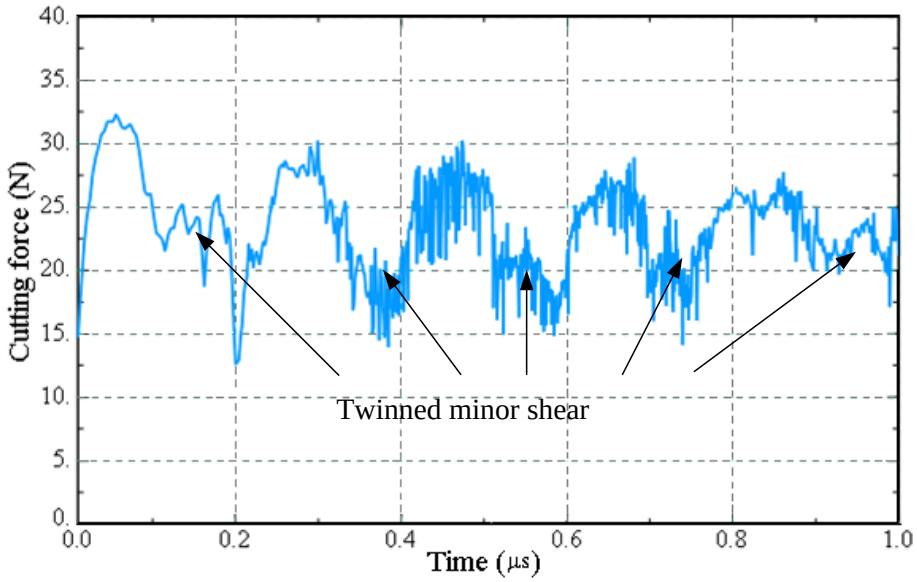

(a)

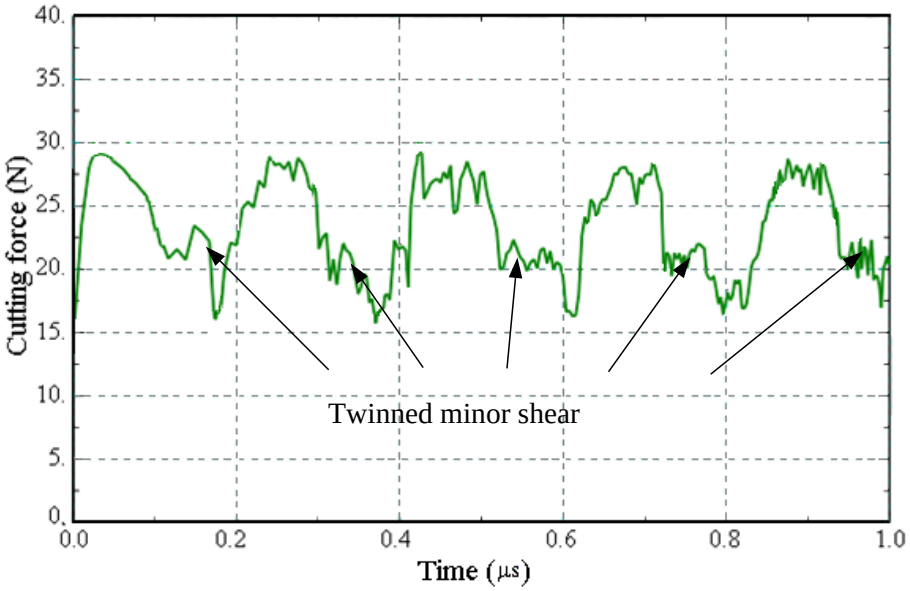

(b)

Figure 7. (a) Simulation result and (b) experiment result on the cutting forces under cutting condition at tool rake angle at 0°, cutting speed at 100 mm/min, and depth of cut at 7μm

4.2 Material removal mechanism

To further learn the unique material removal process in diamond cutting of BMG, the chip formation process was also observed and simulated, as shown in Fig. 9. Fig.9 shows the generated and simulated serrated chip morphologies in diamond cutting of BMG under different rake angles. It should be noted that the original chip formed from the diamond cutting test was a continuous curled chip. Since the cutting distance in the test is relatively long compared to the simulation, the long continuous curled chip was rolled up as a spiral. When the chip length increased, the out curvature of the spiral was decreased.in the zoom-in view. As a result, the magnified view of the chip near the primary deformation zone in SEM like being straightened, as shown in Fig. 8. As shown in Fig. 9, the chips of BMG features the twined shear band, namely a big zigzag followed by a small one, which explains the twined minor shear phenomenon shown in Fig. 7. A good consistency between the experimental and simulated results also validates the simulation can well reflect the chip formation process. From the simulated heat distribution results, it is learned that serrated chips are caused by the adiabatic effect due to the low heat conductivity. Both the experimental and simulation results indicates that a second shearing process generates in the chip formation process, which cause a small zigzag shape following the big one and leads to the cutting force fluctuations during each serrated chip formation cycle.

In addition, Fig.9 shows that the serrated chip is very obvious under the rake angle of 0°, -10° and 25 °, while the serrated chip is unconspicuous at rake angle 5°. It can be inferred that the negative rake angle will increase the serrated

level of chips. In addition, from Fig.9, it can also be seen that the twinned minor shear phenomenon existed in the cycle of each serrated chip. And the larger negative rake angle, the more obvious the twinned shear and the serrated. Therefore, the results of chip comparison proved that the extent of serrated chip is very sensitive to the rake angle. It is worth to note that the material springback and the generated burrs of BMG can lead to the rugged and multifarious topography of the unmachined surfaces in the pictures of figure 9. As the rangeability of the rugged surfaces is much smaller than the cutting depth, the observed experimental results should be reliable. The acceleration and deceleration of the machine tools is very crucial for the quick stop experiments. In the experiments, the experiment setup (Moore Nanotech 350) is working in fast move mode, the maximum allowable acceleration will be imposed on the slides. Although it is hard to exactly estimate the accurate acceleration and deceleration in the experiments, the sudden stop of the feeding slide can be indirectly validated by the experiment results of quick stop experiments, which might be attributed to the relative small cutting speed in the experiments.

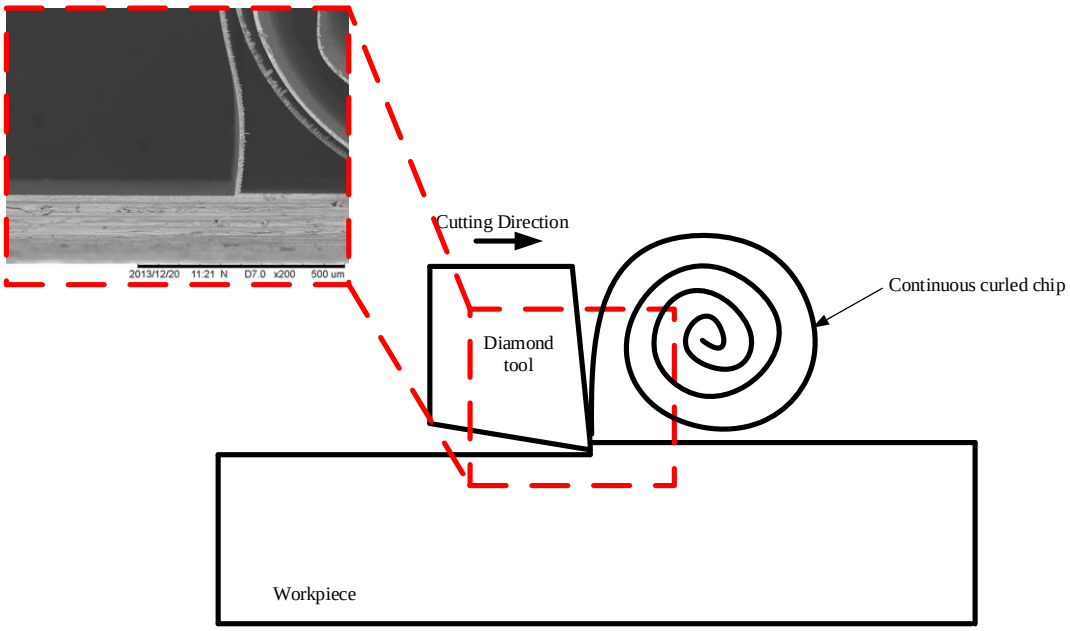

Figure 8. The formation mechanism of the spiral chips.

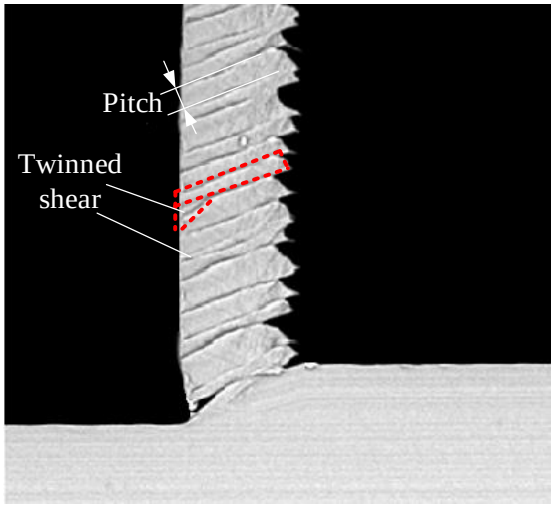

(a1) Chip of test

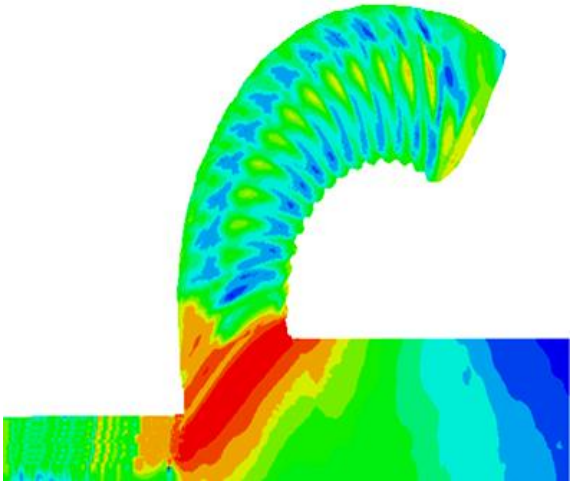

(a2) Chip of simulation

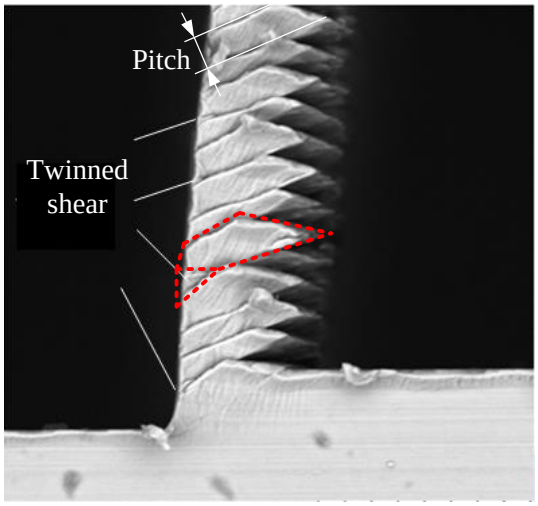

(b1) Chip of test

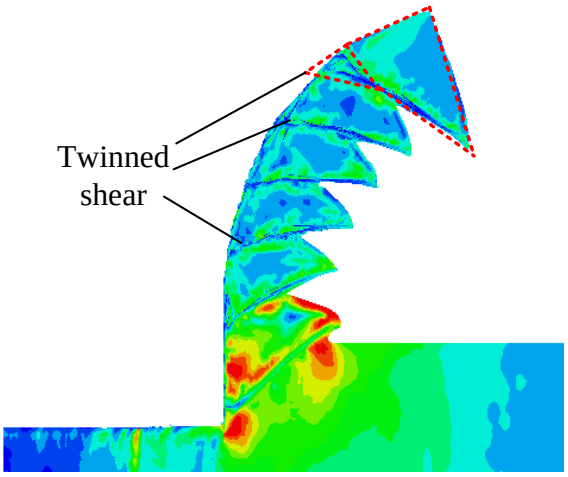

(b2) Chip of simulation

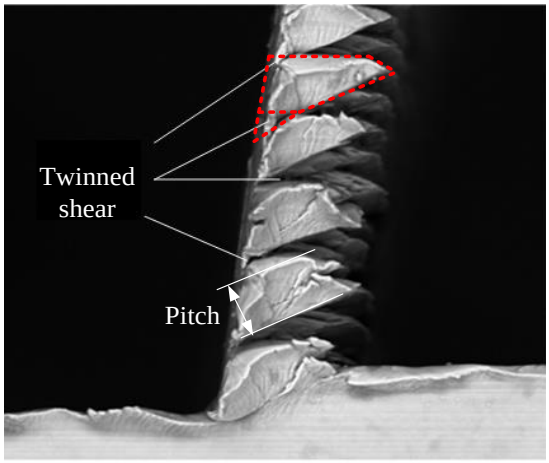

(c1) Chip of test

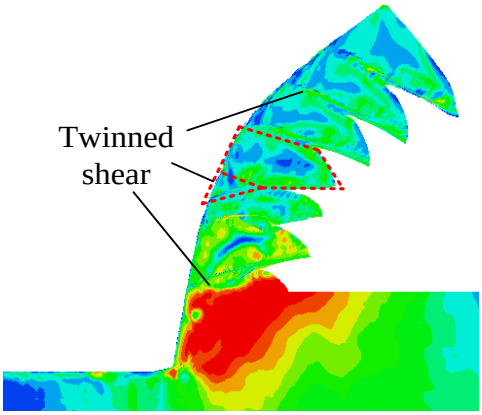

(c2) Chip of simulation

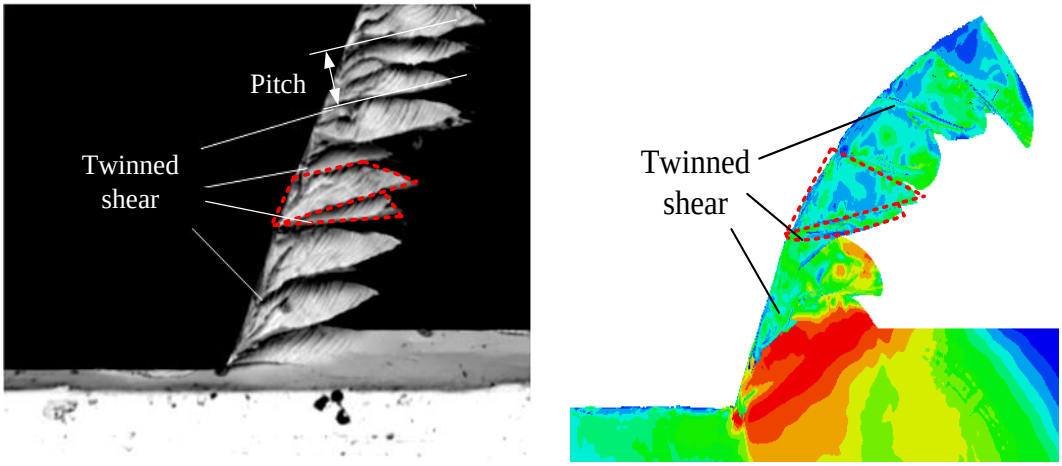

(d1) Chip of test (d2) Chip of simulation

Figure 9. Comparison of chips between experiment and simulation in ultra-precision turning of BMG at different rake angles: (a) 5 °, (b) 0°, (c) -10°, (d) -25°, with cutting condition in cutting speed at 100 mm/min, and depth of cut at 7μm

Fig. 10 is the evaluate model of the extent for the serrated chip of BMG. Table 5 showed the effects of rake angle on the main cutting force and the pitch of the serrated chip in simulations and tests of BMG. The results of simulation agree with the experiment result well. From Table 4, the average value and amplitude of cutting force increased when the tool rake angle changed from the positive to be negative, and the pitch of the serrated chip also has the same rule. So, the results proved that the negative rake angle will increase the extent of the serrate.

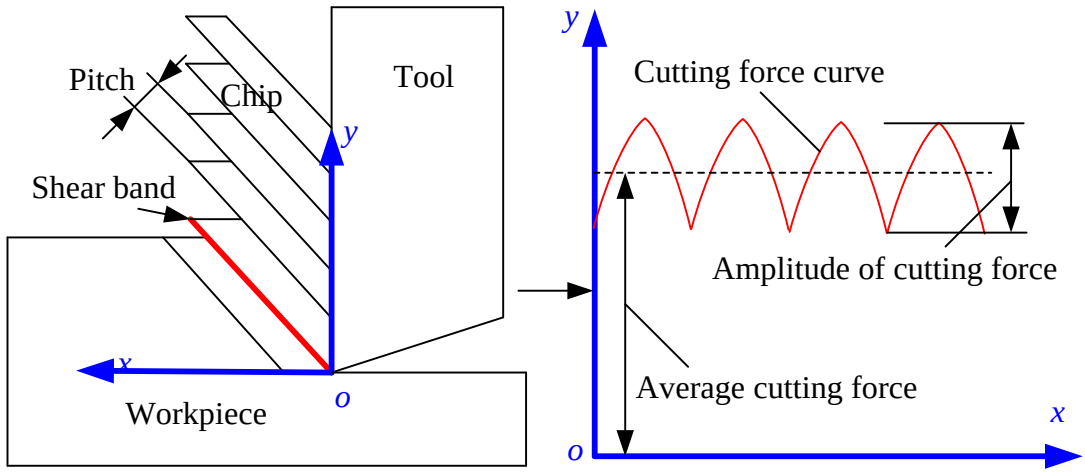

Figure 10. Evaluate model of the extent for the serrated chip of BMG

Instead of the cutting speed at 100 mm/min, the experiment results adopting the different cutting speeds at 200 and 400 mm/min have been added in the revised manuscript. Similar twinned-serrated chips also observed at 200 and 400 mm/min using the -10° tool rake angle, as shown in Fig. 11 (a) and (b), which indicates that the chip formation mechanism is majorly attributed to inherent material properties. A lower cutting depth at 1 μm was also adopted in the experiments to observe the chip formation, as shown in Fig. 11 (c). In this case, even though the chips are characterized

as snatchy shapes compared with the larger cutting depths, the twined chips can also clearly observed. Based on the simulation results, the serrated chips are majorly caused by the adiabatic effect due to the low heat conductivity.

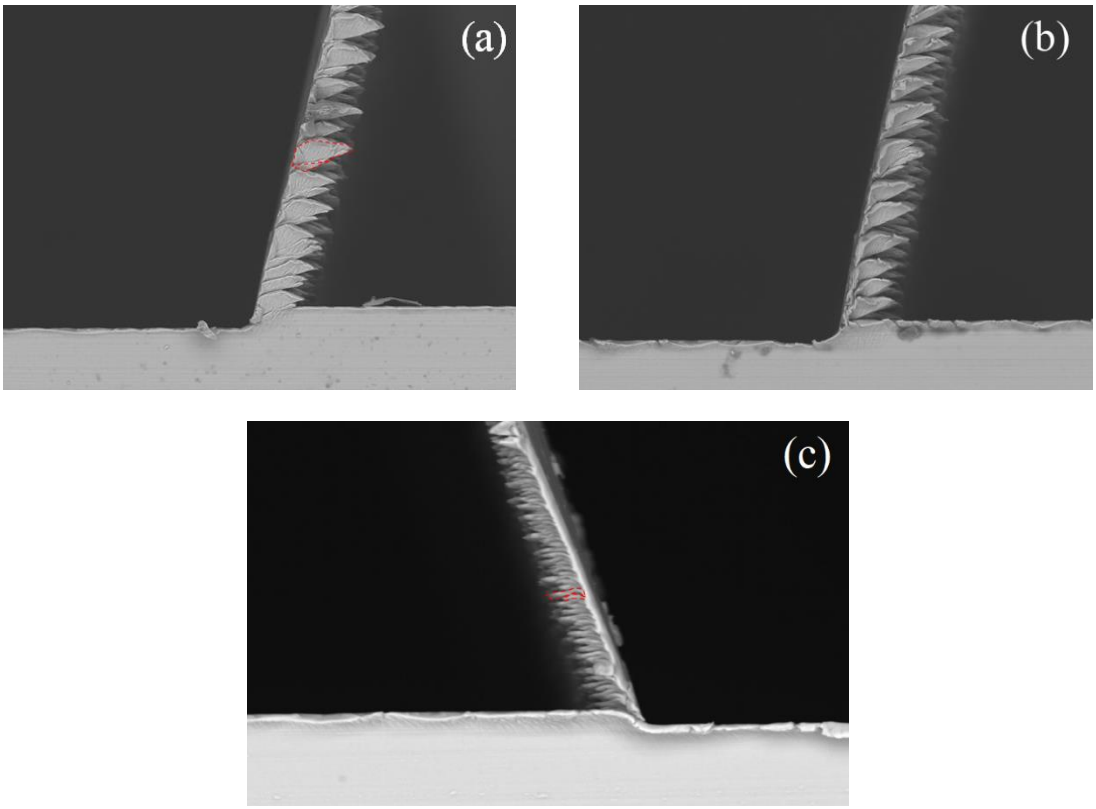

Figure 11. The SEM image of the chip formation with tool rake angle in -10° under cutting conditions in (a) the cutting speed at 200 mm/min and depth of cut in 7μm; (b) the cutting speed 400 mm/min and depth of cut in 7μm; (c) the cutting speed at 100 mm/min and cutting depths at 1 μm

Table 5. Effect of rake angle on cutting force and the pitch of the serrated chip

	Pitch		Average cutting force		Amplitude of the cutting force	
Rake angle	Simulation	Test	Simulation	Test	Simulation	Test
5	2.35 μm	2.64 μm	20.1 N	24.91 N	8.81 N	7.26 N
0	3.32 μm	3.56 μm	23.7N	27.22 N	15.93 N	11.87 N
-10	6.17 μm	6.81 μm	27.3 N	34.09 N	16.24 N	12.18 N
-25	7.05 μm	7.33 μm	32.6 N	38.59 N	17.06 N	13.23 N

5. Conclusions

To investigate the cutting mechanisms of serrated chip formation in ultra-precision micro-cutting (UPMC) of bulk metallic glass (BMG), a series of UPMC tests have been carried out and the cutting process is simulated by finite element

method. The unique twinned-serrated chip formation process in diamond cutting of BMG was first observed using experimental methods, and finite element theory was also used to simulated the chip formation process. The unique effects of the twinned-serrated chips on cutting force oscillations were also analyzed in order to learn the to learn the material mechanism of BMG. The changes of temperature and stress in the cutting zone were learned based on an adiabatic model that calculating the temperatures in the shear band according to the increase of the adiabatic thermal energy caused by the inelastic deformation. The main conclusions of this work can be summarized as follows:

1. The material removal process of BMG is characterized twined minor shear phenomenon in each cycle of each serrated chip formation. The primary shear band is formed majorly due to the material thermal soften effect and the stress in the adiabatic shear band falls rapidly. The twinned minor shear zone blends together with the primary serrated chip due to the press of the tool.
2. The proposed adiabatic model can well simulate the chip formation process of BMG, and validates that the chip formation includes three separate stages: namely elastic deformation, plastic deformation and shear-fracture. Each stage happens along with the change of temperature and stress.
3. serrated chips are caused by the adiabatic effect due to the low heat conductivity. Both the experimental and simulation results indicates that a second shearing process generates in the chip formation process, which cause a small zigzag shape following the big one and leads to the cutting force fluctuations during each serrated chip formation cycle.
4. The average value and amplitude of cutting force increased when the tool rake angle changed from the positive to be negative, and the pitch of the serrated chip also has the same rule. So, the results proved that the negative rake angle will increase the extent of the serrate.

References：

[1] Mustafa Bakkal, Albert J. Shih, Ronald O. Scattergood, Chip formation, cutting forces, and tool wear in turning of Zr-based bulk metallic glass, International Journal of Machine Tools and Manufacture 44 (2004) 915–925.

[2] Mustafa Bakkal, Albert J. Shih, Ronald O. Scattergood, C.T. Liu, Machining of a Zr–Ti–Al–Cu–Ni metallic glass, Scripta Materialia 50 (2004) 583–588.

[3] Hu Huang, Jiwang Yan, Microstructural changes of Zr-based metallic glass during microelectrical discharge machining and grinding by a sintered diamond tool, Journal of Alloys and Compounds 688 (2016) 14–21.

[4] Mustafa Bakkal, Chain T. Liu, Thomas R. Watkins,Ronald O. Scattergood, Albert J. Shih, Oxidation and crystallization of Zr-based bulk metallic glass due to machining, Intermetallics 12 (2004) 195–204.

[5] Minqiang Jiang, Lanhong Dai, Formation mechanism of lamellar chips during machining of bulk metallic glass, Acta Materialia 57 (2009) 2730–2738.

[6] Kazutaka Fujita, Yasuo Morishita, Nobuyuki Nishiyama,Hisamichi Kimura and Akihisa Inoue, Cutting characteristics of bulk metallic glass, Materials Transactions 46 (2005) 2856–2863.

[7] James Zhu, Hyun Jin Kim, Shiv G. Kapoor, Microscale drilling of bulk metallic glass, Journal of Micro and Nano-Manufacturing 1 (2013) 041004-1–9.

[8] Mustafa Bakkal, Albert J. Shih, Samuel B. McSpadden, Ronald O. Scattergood, Thrust force, torque, and tool wear in drilling the bulk metallic glass, International Journal of Machine Tools and Manufacture 45 (2005) 863–872.

[9] Mustafa Bakkal, Albert J. Shih, Samuel B. McSpadden, C.T. Liu, Ronald O. Scattergood, Light emission, chip morphology, and burr formation in drilling the bulk metallic glass, International Journal of Machine Tools and Manufacture 45 (2005) 741–752.

[10] Huo, Dehong. Micro-cutting: fundamentals and applications. John Wiley & Sons, 2013.

[11] Xiao Chen , Junfeng Xiao , Yan Zhu , Ruiji Tian , Xuewen Shu , Jianfeng Xu, Micro-machinability of bulk metallic glass in UPMC, Materials and Design 136 (2017) 1–12.

[12] Dongxue Han, Gang Wang, Jinfu Li, K.C. Chan, Suet To, Fu Fa Wu, Yu Lai Gao, Qi Jie Zhai, Cutting Characteristics of Zr-Based Bulk Metallic Glass, Journal of Materials Science and Technology 31 (2015) 153–158.

[13] Guang Chen, Chengzu Ren, Pan Zhang, Kuihu Cui, Yuanchen Li, Measurement and finite element simulation of micro-cutting temperatures of tool tip and workpiece, International Journal of Machine Tools and Manufacture 75 (2013) 16–26.

[14] Tugrul Özel, The influence of friction models on finite element simulations of machining, International Journal of Machine Tools and Manufacture 46 (2006) 518–530.

[15] Maryam Mahnama, Mohammadreza Movahhedy, Prediction of machining chatter based on FEM simulation of chip formation under dynamic conditions, International Journal of Machine Tools and Manufacture 50 (2010) 611–620.

[16] Chengyong Wang, Feng Ding, Dewen Tang, Lijuan Zheng, Suyang Li, Yingxing Xie, Modeling and simulation of the high-speed milling of hardened steel SKD11 (62 HRC) based on SHPB technology, International Journal of Machine Tools and Manufacture 108 (2016) 13–26.

[17] Gordon R. Johnson, William H. Cook, A constitutive model and data for metals subjected to large strains high strain rates and high temperatures, In Proceeding of the 7th International Symposium on Ballistics, Hague, Netherlands, 21 (1983) 541–547.

[18] Weihua Yin (2013). Compressive behavior of bulk metallic glass under different conditions — Coupled effect of temperature and strain rate (PhD dissertation). Available from ProQuest Dissertations and Theses database. (UMI No. 3608533)

[19] Gordon R. Johnson, William H. Cook, Fracture characteristics of three metals subjected to various strains, strain rates, temperatures and pressures, Engineering Fracture Mechanics 21 (1985) 31-48.